Tubular cell-enriched subpopulation of primary renal cells improves survival and augments kidney function in rodent model of chronic kidney disease

Rusty Kelley, Eric S. Werdin, Andrew T. Bruce, Sumana Choudhury, Shay M. Wallace, Roger M. Ilagan, Bryan R. Cox, Patricia Tatsumi-Ficht, Elias A. Rivera, Thomas Spencer, H. Scott Rapoport, Belinda J. Wagner, Kelly Guthrie, Manuel J. Jayo, Timothy A. Bertram and Sharon C. Presnell

Am J Physiol Renal Physiol 299:F1026-F1039, 2010. First published 8 September 2010; doi:10.1152/ajprenal.00221.2010

Am J Physiol Renal Physiol 299: F1026–F1039, 2010.
First published September 8, 2010; doi:10.1152/ajprenal.00221.2010.

Tubular cell-enriched subpopulation of primary renal cells improves survival and augments kidney function in rodent model of chronic kidney disease

Rusty Kelley, Eric S. Werdin, Andrew T. Bruce, Sumana Choudhury, Shay M. Wallace, Roger M. Ilagan, Bryan R. Cox, Patricia Tatsumi-Ficht, Elias A. Rivera, Thomas Spencer, H. Scott Rapoport, Belinda J. Wagner, Kelly Guthrie, Manuel J. Jayo, Timothy A. Bertram, and Sharon C. Presnell

Tengion, Incorporated, Science and Technology, Winston-Salem, North Carolina

Submitted 19 April 2010; accepted in final form 28 August 2010

Kelley R, Werdin ES, Bruce AT, Choudhury S, Wallace SM, Ilagan RM, Cox BR, Tatsumi-Ficht P, Rivera EA, Spencer T, Rapoport HS, Wagner BJ, Guthrie K, Jayo MJ, Bertram TA, Presnell SC. Tubular cell-enriched subpopulation of primary renal cells improves survival and augments kidney function in rodent model of chronic kidney disease. *Am J Physiol Renal Physiol* 299: F1026–F1039, 2010. First published September 8, 2010; doi:10.1152/ajprenal.00221.2010.—Established chronic kidney disease (CKD) may be identified by severely impaired renal filtration that ultimately leads to the need for dialysis or kidney transplant. Dialysis addresses only some of the sequelae of CKD, and a significant gap persists between patients needing transplant and available organs, providing impetus for development of new CKD treatment modalities. Some postulate that CKD develops from a progressive imbalance between tissue damage and the kidney's intrinsic repair and regeneration processes. In this study we evaluated the effect of kidney cells, delivered orthotopically by intraparenchymal injection to rodents 4–7 wk after CKD was established by two-step 5/6 renal mass reduction (NX), on the regeneration of kidney function and architecture as assessed by physiological, tissue, and molecular markers. A proof of concept for the model, cell delivery, and systemic effect was demonstrated with a heterogeneous population of renal cells (UNFX) that contained cells from all major compartments of the kidney. Tubular cells are known contributors to kidney regeneration in situ following acute injury. Initially tested as a control, a tubular cell-enriched subpopulation of UNFX (B2) surprisingly outperformed UNFX. Two independent studies (3 and 6 mo in duration) with B2 confirmed that B2 significantly extended survival and improved renal filtration (serum creatinine and blood urea nitrogen). The specificity of B2 effects was verified by direct comparison to cell-free vehicle controls and an equivalent dose of non-B2 cells. Quantitative histological evaluation of kidneys at 6 mo after treatment confirmed that B2 treatment reduced severity of kidney tissue pathology. Treatment-associated reduction of transforming growth factor (TGF)-β1, plasminogen activator inhibitor (PAI)-1, and fibronectin (FN) provided evidence that B2 cells attenuated canonical pathways of profibrotic extracellular matrix production.

regeneration; stabilization

CHRONIC KIDNEY DISEASE (CKD) affects more than 19 million people in the U.S. and frequently develops as a consequence of chronic obesity, diabetes, and/or hypertension (42). Patients in stage 4–5 CKD receive dialysis and a complex drug regimen, and the number of kidneys available for transplant is vastly insufficient to meet the need (30). New treatments that delay or reduce dialysis dependence are needed to fill this void.

Address for reprint requests and other correspondence: S. C. Presnell, Tengion, Inc., 3929 Westpoint Blvd., Suite G, Winston-Salem, NC 27103 (e-mail: sharon.presnell@tengion.com).

Kidney tissue is composed of >20 specialized cell types structurally organized into morphologically and functionally distinct compartments that act in concert to filter blood, produce urine, and regulate endocrine function and acid-base and electrolyte balance. Cell-cell interactions are critical to kidney function and are at least partially dependent on spatial and architectural relationships. Regenerative approaches to CKD aim to reestablish homeostasis in part through restoration of cellular organization and intercellular communication.

One approach to identifying candidate treatments for regenerating organ function is to select native organ-specific cells that possess relevant bioactivity; however, the therapeutic effect of native renal cells isolated from kidney tissue as primary cultures has not been tested in established progressive models of CKD. In this study, recently published methods for isolating and expanding heterogeneous cultures of primary renal cells (1, 15) were used to establish unfractionated (UNFX) cultures containing cells from all major compartments of the kidney. Methods were adapted to enable postculture production of an enriched epithelial cell subpopulation of UNFX comprising predominantly cells from the tubular and collecting duct systems (B2) and relatively depleted of glomerular, vascular, and erythropoietin-producing cells.

Two-step 5/6 nephrectomy (NX) in rats reproducibly generates terminally progressive renal failure with characteristic systemic and histological parameters of CKD [e.g., hypertension, reduced glomerular filtration rate (GFR), elevated serum creatinine (sCREAT) and blood urea nitrogen (BUN), glomerular and tubulointerstitial fibrosis, hyperlipidemia, hyperphosphatemia, and anemia] (3, 17, 26, 29). The clinically relevant features of the NX model combined with technical reproducibility and commercial availability provided the basis for its selection as the disease model for these studies.

Proof of concept for evaluating in vivo bioactivity (e.g., criteria for treatment initiation, primary in vivo indicators, quantitation of delivered cell persistence) was established with UNFX cells. A 6-mo study with two doses of UNFX was initiated with renal filtration, erythroid homeostasis, and survival as primary indicators. The B2 subfraction was included initially as a less heterogeneous control and surprisingly outperformed UNFX across all primary indicators. The in vivo bioactivity of B2 was confirmed in NX rodents in an independent study, and the specificity of B2 was demonstrated by comparison to both cell-free controls and non-B2 cell controls isolated from the same UNFX preparation. In vitro characteristics and in vivo performance of UNFX and B2 in the rodent CKD model across a spectrum of clinical parameters and potential mechanisms of action for B2's in vivo bioactivity are presented.

Table 1. *Antibodies used in fluorescence-activated cell sorting, immunofluorescence, and immunoblotting experiments*

Step	Antibody	Manufacturer (catalog no.)	Used for (concn.)
Primary	CK8/18/19 (mouse IgG1)	Abcam (ab41825)	FACS (1 μg/ml)
	E-cadherin (mouse IgG2a)	BD Biosciences (610182)	FACS (1 μg/ml)
	PECAM (mouse IgG1)	BD Biosciences (555025)	FACS (1 μg/ml)
	GGT1 (rabbit IgG)	Santa Cruz (sc-20638)	FACS (1 μg/ml)
	Aquaporin 2 (rabbit IgG)	Abcam (ab64154)	FACS (1 μg/ml)
	Cubilin (goat IgG)	Santa Cruz (sc-20609)	IF (5 μg/ml)
	PAI-1 (mouse IgG1)	BD Biosciences (612025)	IB (12.5 μg/ml)
	FN (mouse IgG1)	R&D Systems (MAB1918)	IB (25 μg/ml)
	β-Actin (mouse IgG1)	Sigma (A5441)	IB (10 μg/ml)
Isotype Control	Mouse IgG1	DAKO (X0931)	FACS (1 μg/ml)
	Mouse IgG2a	DAKO (X0932)	FACS (1 μg/ml)
	Rabbit IgG	Invitrogen (02-1202)	FACS (1 μg/ml)
Secondary (detection)	Goat anti-mouse IgG1 (A_{488})	Invitrogen (A21121)	FACS (1 μg/ml)
	Goat anti-mouse IgG2a (A_{488})	Invitrogen (A21131)	FACS (1 μg/ml)
	Chicken anti-rabbit IgG (A_{488})	Invitrogen (A21441)	FACS (1 μg/ml)
	Donkey anti-goat IgG (A_{488})	Invitrogen (A11055)	IF (5 μg/ml)
	Goat anti-rabbit (HRP)	Zymed (81-6120)	IB (1 μg/ml)
	Rabbit anti-mouse (HRP)	Zymed (61-0120)	IB (1 μg/ml)

FACS, fluorescence-activated cell sorting; IF, immunofluorescence; IB, immunoblotting; PECAM, platelet endothelial cell adhesion molecule; GGT1, γ-glutamyl transpeptidase 1; PAI-1, plasminogen activator inhibitor-1; FN, fibronectin; HRP, horseradish peroxidase.

MATERIALS AND METHODS

Cell Isolation and Preparation

UNFX cells were prepared from rodent kidneys as described previously (1). In brief, whole kidneys were harvested from 5-wk-old male Lewis rats (Hilltop Labs, Scottsdale, PA) and dissociated enzymatically in a buffer containing 4.0 U/ml dispase (Stem Cell Technologies, Vancouver, BC, Canada) and 300 U/ml collagenase IV (Worthington Biochemical, Lakewood NJ). Red blood cells (RBCs) and debris were removed from the initial cell suspension by centrifugation through 15% iodixanol (OptiPrep, Axis Shield, Norton, MA). Cells were seeded onto tissue culture-treated polystyrene plates (NUNC, Rochester, NY) and cultured in a 1:1 mixture of high-glucose DMEM and keratinocyte serum-free medium (KSFM) containing 5% (vol/vol) FBS, 2.5 μg of EGF, 25 mg of bovine pituitary extract (BPE), 1× insulin-transferrin-sodium selenite medium supplement (ITS), and antibiotic-antimycotic (all from Invitrogen, Carlsbad CA). Where indicated, outer membranes of UNFX cells were labeled with PKH26 (Sigma catalog no. PKH26GL) according to manufacturer protocol. Before postculture cell separation, UNFX primary cultures were transferred from atmospheric oxygen conditions (21%) to a more physiologically relevant low-oxygen (2%) environment for 24 h, which improved cell separation efficiency and enabled greater detection of hypoxia-induced markers. Postculture UNFX cell suspensions, prepared as 75×10^6 cells in 2 ml of unsupplemented KSFM (uKSFM) were separated on four-step iodixanol [OptiPrep; 60% (wt/vol) in uKSFM] density gradients layered as 16%, 13%, 11%, and 7% iodixanol in 15-ml conical polypropylene tubes and centrifuged at 800 *g* for 20 min at room temperature (without brake). Cellular subfractions were collected after centrifugation as four distinct bands (B1–B4) and a pellet (B5) and washed three times in sterile phosphate-buffered saline (PBS) before use. FACS Aria (Becton Dickinson, Franklin Lakes, NJ) was used for cell characterization via immunocytometry, and data were analyzed with FlowJo (Tree Star) software. Antibodies are listed in Table 1.

mRNA Quantitation

Expression levels of target mRNAs were examined via quantitative real-time PCR (qRT-PCR) using Taqman probes and primer sets (Table 2) and an ABI-Prism 7300 Real Time PCR System (Applied Biosystems, Carlsbad, CA). Samples were homogenized with Qia Shredder, and RNA was isolated with RNeasy Plus Mini Kits (Qiagen, Valencia, CA). cDNA was synthesized with the SSIII VILO kit (Invitrogen). Amplification was performed with the TaqMan Gene Expression Master Mix (Applied Biosystems), with Peptidylprolyl isomerase B (Ppib) as an endogenous control.

Detection of Y Chromosome in Kidney Tissue

Frozen sections (10-μm thickness) were fixed in 1:1 acetone-methanol for 7 min and denatured in 70% formamide prepared in sodium citrate buffer at 65°C for 5 min. Denatured probes (Rat 12/Y Dual Paint no. 1631, Cambio, Cambridge, UK) were hybridized overnight and washed five times in 50% formamide-2× SSC at 42°C. Labeled sections were preserved and counterstained in a 1:10 mixture of Fluorsave (EMD Chemicals, Gibbstown, NJ) and Vecto/DAPI (Vector Labs, Burlingame, CA) and visualized via fluorescent microscopy. Inclusion of the chromosome 12 probe (FITC, green) allowed distinction between binding of the Y probe to the Y chromosome (Cy3, red) and binding of the Y probe to homologous regions of the chromosome 12 short arm and centromere (Y red + 12 green = yellow/orange).

Sex-Determining Region Y Gene Detection

Primer Express 3.0 software was used to design custom primers for Sex-determining region Y (*SRY*) AAGCGCCCCATGAATGC (forward), AGCCAACTTGCGCCTCTCT (reverse), and TTTATGGT-

Table 2. *RT-PCR probes*

Gene	Taqman Assay
E-cadherin	Rn00580109_m1
Cubilin	Rn00584200_m1
Nephrin	Rn00575235_m1
Erythropoietin	Rn01481376_m1
KDR	Rn00564986_m1
TGFb1	Rn00572010_m1
PAI-1	Rn00561717_m1
FN	Rn00569575_m1
Aqp2	Rn00563755_m1
Aqp4	Rn00563196_m1
Hes1	Rn00577566_m1
CD68	Rn01495632_g1
PECAM	Rn01467262_m1

Table 3. *Histological scoring: composite score parameters and scoring system used*

Composite Score	Parameters Evaluated for Composite Score	Scoring
Tubulointerstitial injury score (TIS)	Tubular casts	Standard scoring
	Tubular atrophy	
	Interstitial fibrosis	
	Tubular hyperplasia	
	Tubular hypertrophy	
	Basement membrane thickness	
Glomerular injury score (GIS)	Mesangial sclerosis and/or hyalinosis	
	Thickening of Bowman's capsule	
	Glomerular tuft atrophy/collapse	
	Glomeruli area (mm^2)/no. of glomeruli per field	GArea/#

Scoring system is explained in Table 4.

GTGGTCCCGTG-MGB (probe). Genomic DNA was isolated with the DNeasy Blood and Tissue kit (Qiagen) for PCR amplification. Data were evaluated with Applied Biosystems Relative Quantitation (RQ) software.

Western Blotting

Tissues were lysed in buffer containing 50 mM Tris pH 7.5, 150 mM NaCl, 0.5% NP-40, and protease inhibitor (Roche). Twenty-microgram protein samples were electrophoresed through 10% PAGE gel with 1× MES running buffer (Invitrogen) and transferred to nitrocellulose membrane with an iBLOT Dry Blotting System (Invitrogen). Membranes were blocked with 5% low-fat milk dissolved in TBST (20 mM Tris·HCl pH 7.5, 150 mM NaCl, 0.1% Tween) for 1 h, probed with primary antibody (Table 1) diluted in blocking buffer overnight at 4°C and the appropriate secondary antibody (Table 1) for 1 h, and then developed with the ECL Advance Western Blot Detection Kit (Thermo Scientific).

Functional Assays

γ-Glutamyl transpeptidase activity. An assay for γ-glutamyl transpeptidase (GGT)1 activity was adapted from a previously published method (40) in which nitroaniline produced by GGT1 activity is proportional to absorbance at 405 nm (A_{405}). One hundred thousand cells were incubated with 2.5 mM L-glutamic acid γ-*p*-nitroanilide (Sigma) in Tris·HCl pH 8.6 containing 150 mM NaCl and 50 mM glycylglycine (200 μl) for 1 h at room temperature. A_{405} readings were corrected with reagent blank, and LLC-PK1 cells (American Type Culture Collection) served as the positive control.

Albumin uptake. These procedures were adapted from published methods (4, 46). Culture medium of cells grown to confluence in 24-well collagen IV plates (BD Biocoat) was replaced for 18–24 h with phenol red-free, serum-free, low-glucose DMEM (pr−/s−/lg DMEM) containing 1× antimycotic-antibiotic and 2 mM glutamine. Immediately before assay, cells were washed and incubated for 30 min with pr−/s−/lg DMEM with (in mM) 10 HEPES, 2 glutamine, 1.8 $CaCl_2$, and 1 $MgCl_2$. Cells were exposed to 25 μg/ml rhodamine-conjugated bovine albumin (Invitrogen) for 30 min, washed with ice-cold PBS to stop endocytosis, and fixed immediately with 2% paraformaldehyde containing 25 μg/ml Hoechst nuclear dye. For inhibition experiments, 1 μM receptor-associated protein (RAP) (Ray Biotech, Norcross, GA) was added 10 min before albumin addition (46). Microscopic imaging and analysis were performed with a BD Pathway 855 High-Content BioImager (Becton Dickinson).

CKD Model

5/6 Nephrectomized (2-step) female Lewis rats were obtained from Charles River Laboratories.

Animal care. All procedures involving animals were conducted in accordance with National Institutes of Health guidelines and were approved by the Institutional Animal Care and Use Committee of Research Triangle Institute, International (Research Triangle Park, NC), where all animal studies were conducted. Rats were anesthetized, and remnant kidneys were exposed via ventral medial-lateral incision. Cells were suspended in 100-μl sterile PBS, loaded into a 1-ml syringe fitted with a ½-in. 23-gauge needle (Becton Dickinson), and delivered directly to the kidney through the apical cortex at a depth of ~3–5 mm (for diagram of injection site, see Fig. 6*A*). In *studies A* and *B*, cells were delivered to rats 6–12 h after cell harvest (see Fig. 3*C* for treatment groups and dose administration in *studies A* and *B*). In *study B′*, the following treatment groups were appended: *1*) additional B2 rats ($n = 5$) delivered at 5×10^6, generated from an independent preparation of UNFX; *2*) non-B2 cells ($n = 5$), delivered at 5×10^6, isolated from the same UNFX preparation, with the non-B2 cell mixture generated by combining two of the adjacent bands (B3 and B4) produced by the density-gradient centrifugation protocol; and *3*) cell-free vehicle controls ($n = 4$), comprising injection diluent (sterile PBS). In *study B′*, all treatments were delivered 18–24 h after cell harvest to better approximate a feasible clinical scenario (i.e., a time frame compatible with overnight shipment).

In-life analysis. Body weight was recorded weekly. Blood and serum samples were collected biweekly via tail vein or orbital bleed. Serum BUN, sCREAT, hematocrit (Hct), and RBC number were measured weekly by a qualified commercial vendor (Antech Diagnostics). Full clinical chemistry and hematology panels were run at baseline, midpoint, and necropsy and enabled quantification of serum albumin (sALB), A-to-G ratio (A:G), hemoglobin, phosphorous, and calcium as reported. Animals were killed at study end point or when so ordered by the study veterinarian. At necropsy, kidneys were weighed and tissues collected for histology and analysis.

Postnecropsy analyses. Kidneys were bisected longitudinally. One half was serially sectioned (transverse, 10 μm) to generate samples for gDNA, RNA, and protein. Sections were collected from cortex through medullary zone and into the renal pelvis. Paraffin-embedded 5-μm tissue sections were stained with Masson's trichrome and periodic acid Schiff (PAS) by standard procedures. Evaluation of remnant kidney parenchyma was performed by light microscopy. Tubulointerstitial and glomerular injury indexes were scored with standard semiquantitative grading scales (35, 37) of 0–4 (examined at a high-power field) and the parameters outlined in Tables 3 and 4.

Morphometry

Low- and high-power digital images of sections representing both intact and remnant kidney sections were captured from two or three different sites of kidney parenchyma with a Nikon Digital Camera (DS-U1) mounted on a Nikon microscope (Eclipse 50i). Digital images were color-printed on regular 8.5 × 11-in. paper and labeled with section identification (animal no., treatment, site, stain, and magnification). Low-power images were used to assess tubular dilatation, atrophy, glomerular number (count), and corticomedullary distribution, using the arcuate artery and the kidney capsule as two points of reference.

Table 4. *Histological scoring: score system values*

Score	Standard Scoring (evaluated semiquantitatively as % change from normal)	GArea/# (calculated from morphometric analysis of glomeruli area and no. per field)
0	Normal histology, no change	>2.5 to ≤5.0
1	Minimal changes, <25%	>5.0 to ≤8.0
2	Mild changes, 25–50%	>8.0 to ≤10.0
3	Moderate changes, 50–75%	>10.0 to ≤12.5
4	Marked changes, >75%	>12.50 to ≤20.0

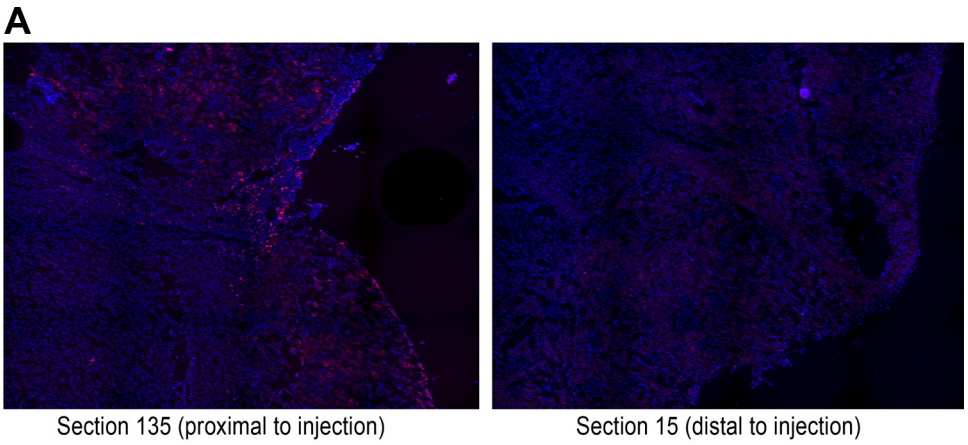

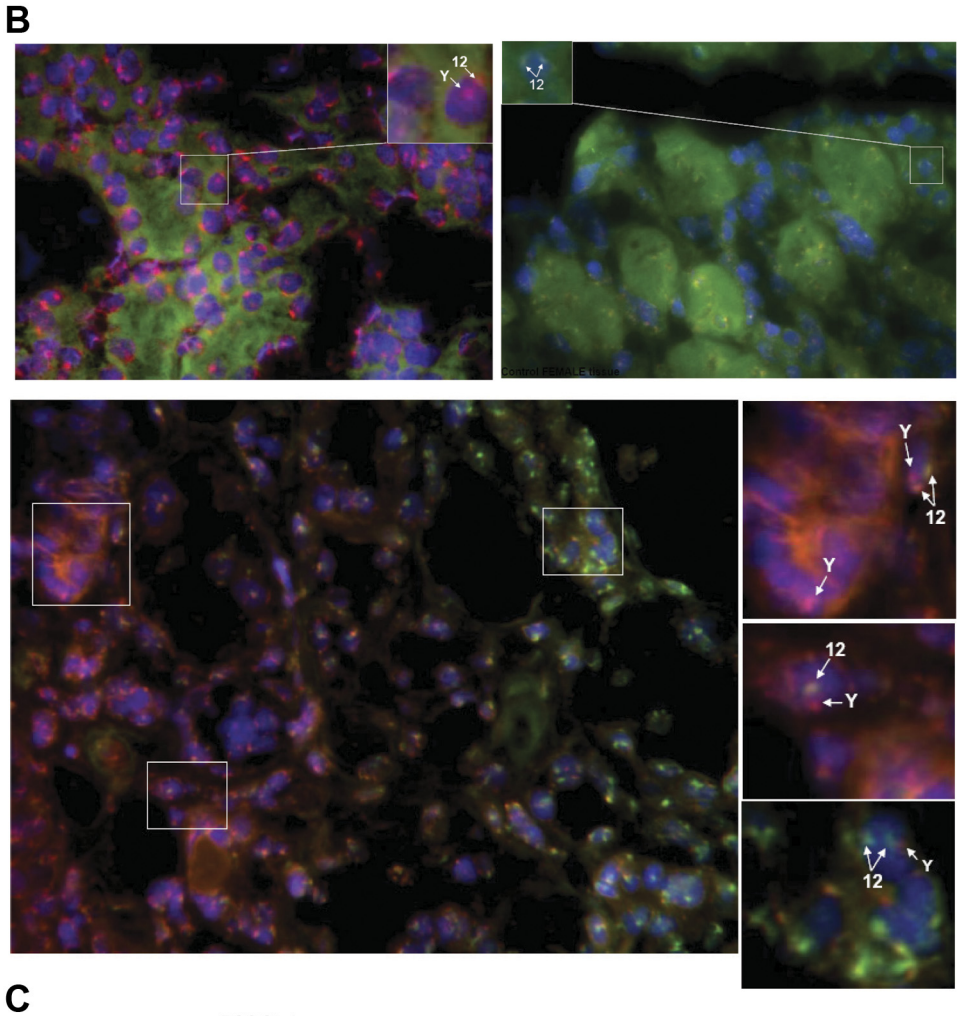

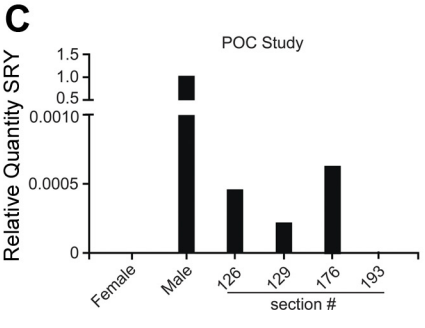

Fig. 1. Detection of implanted cells in host kidney. Retention of 10^7 male UNFX donor cells labeled with PKH26 (red) was assessed at 4 wk after injection into the remnant kidney of a female 2-step 5/6 nephrectomy (NX) recipient. *A*: fluorescence microscopy detection of red PKH26-labeled cells in frozen sections proximal to (section 135) and distal to (section 15) the estimated injection site (nuclei counterstained blue with DAPI). *B*: detection of donor cells in situ by fluorescent in situ hybridization (FISH) using probes for Y and 12 chromosomes (Cy3/FITC) 3 mo after implantation. Green cytoplasm = tubular cell autofluorescence; blue = nuclei (DAPI counterstain). *Top left*: control male tissue showing the presence of Y chromosome (red dots) in nuclei along with chromosome(s) 12 (yellow/orange dots generated by binding of both Y and 12 probes). *Top right*: control female tissue showing labeled chromosomes 12 (nuclear, green dots). *Bottom*: female recipient implanted with male cells, showing Y chromosome+ cells present in the female tissue. *Insets* highlight representative cells stained for both Y chromosome (red) and chromosome 12 (orange). *C*: PCR-based detection of the male-specific Sex-determining region Y (*SRY*) gene in genomic DNA isolated from serially sectioned remnant kidney tissue collected proximal to (sections 126, 129, and 176) or distal to (section 193) the estimated injection site. Unmanipulated female and male kidney tissues were included as negative and positive controls, respectively. POC, proof of concept.

Table 5. *Effect of UNFX in proof-of-concept study*

	Pretreatment		12 wk Posttreatment		
Assessment	Sham NX	NX	Sham NX	NX*	UNFX (10^7)
BUN, mg/dl	23.5 ± 2.1	51.6 ± 5.5	17.5 ± 2.3	104 ± 2.6	65.5 ± 16
sCREAT, mg/dl	0.5 ± 0.1	1.0 ± 0.0	0.5 ± 0.1	2.6 ± 0.2	1.5 ± 0.6
Hct, %	45.4 ± 2.3	41.8 ± 1.5	46.3 ± 0.7	35.2 ± 1.9	36.8 ± 7.1
RBC, × 10^6/μl	8.3 ± 0.3	8.0 ± 0.4	7.8 ± 0.6	6.3 ± 0.5	6.6 ± 1.2

Key parameters of renal filtration [serum creatinine (sCREAT) and blood urea nitrogen (BUN)] and erythropoiesis [hematocrit (HCT) and red blood cell count (RBC)] were tracked in 2-step 5/6 nephrectomy (NX) and Sham NX rats before and after treatment with UNFX cells. *NX rats did not survive to 12 wk; values reported were calculated from preterminal blood draws.

Statistics

One-way analysis of variance (ANOVA) was performed on serum chemistry results from all 10- to 20-wk data (Fig. 5) with JMP version 7.0 from SAS Institute Inc (Cary, NC). Statistical significances were determined by an unpaired *t*-test with a two-tailed *P* value with GraphPad Prism software (Figs. 4, 5, 7–9).

RESULTS

Proof-of-Concept Pilot Studies

Cell delivery and posttreatment detection. Male UNFX donor cells were detectable within the remnant kidney of the NX female recipient host at 4 wk after implant, as evidenced by visualization of PKH26 dye-labeled cells within the parenchyma adjacent to the injection site (Fig. 1*A*). Retention of donor cells at the 3 mo time point was verified in frozen tissue sections by fluorescent in situ hybridization (FISH) with rat Y/12 chromosome probes (Fig. 1*B*), confirming the presence of male donor cells in tubular and peritubular regions, predominantly localized within the corticomedullary zone. Finally, detection of the male-specific *SRY* gene by PCR in serial tissue sections supported the Y-chromosome FISH findings and provided the basis for semiquantitative evaluation of donor cell retention in subsequent studies (Fig. 1*C*).

UNFX effects on renal function at 12 wk after treatment. Before treatment, commercially obtained NX rats were characterized by ≥200% increases in sCREAT and BUN and mildly depressed Hct at 9 wk after completion of the two-step 5/6 nephrectomy procedures performed by the vendor compared with age- and sex-matched healthy rats that underwent sham nephrectomy procedures (Sham NX) (Table 5). Notably, both UNFX-treated rats survived to study completion (12 wk after treatment), whereas none of the three untreated NX control animals survived (mean survival of NX rats was 48 ± 29 days). Consistent with the survival results, systemic parameters of renal function, as measured by serum chemistries of prenecropsy blood samples obtained from UNFX, NX, and Sham NX rats, showed positive effects of UNFX treatment (Table 5).

B2 is a Tubular Cell-Enriched Subpopulation of UNFX

Although UNFX contains a large proportion of tubular cells, it is a heterogeneous population, harboring cells from all major compartments of the kidney and some undefined cell types. We postulated that the in vitro (1, 15) and in vivo (Table 5) bioactivities of UNFX could be contingent on its inherent heterogeneity, so we sought to include a more homogeneous population of tubular cells as a comparative control. UNFX cultures were harvested and subfractionated with discontinuous density gradients. The B2 subpopulation reproducibly sedimented in the 1.045–1.063 g/ml range and represented ~50% of the UNFX cell input (52.0% ± 14.4 based on 5 independent preparations).

Population-based protein expression profiles were generated from five independent preparations (Table 6) and indicated that B2, while heterogeneous, was predominantly epithelial and enriched for cells of the tubules and collecting ducts as evidenced by the percentage of cells expressing E-cadherin, cytokeratins 8, 18, and 19 (CK8/18/19), GGT1, and aquaporin 2 (24, 25, 34, 39, 41), although a small fraction of endothelial cells remained, as evidenced by the percentage of cells expressing platelet endothelial cell adhesion molecule (PECAM) (7). Relative enrichment (calibrated to UNFX; RQ = 1), for

Table 6. *Phenotypic characterization of B2 by flow cytometry*

Marker	Marker-Positive B2 cells, %
E-cadherin	88.05 ± 5.14
CK8/18/19	83.54 ± 0.72
GGT1	52.09 ± 5.65
Aquaporin 2	48.24 ± 5.35
PECAM	1.41 ± 0.23

Values are means ± SD for 5 preparations. Five independent preparations of B2 cells were generated from 5 independent preparations of UNFX cells and subjected to quantitative flow cytometric analysis with general epithelial markers [E-cadherin, cytokeratins 8, 18, and 19 (CK8/18/19)], a tubular cell marker (GGT1), a collecting duct marker (aquaporin 2), and an endothelial cell marker (PECAM).

Table 7. *Comparative gene expression analysis of B2 (tubular enriched) and B4 (non-tubular enriched) cells*

	Expression Relative to UNFX		
Marker	B2	B4	B2-to-B4 Gene Expression Ratio
E-cadherin	21.2 ± 0.1	12.8 ± 0.1	1.66
Cubilin	16.5 ± 0.1	5.5 ± 0.1	3.00
Nephrin	0.9 ± 0.1	207.3 ± 0.8	0.00
Erythropoietin	1.1 ± 0.0	3.8 ± 0.1	0.29
KDR	0.4 ± 0.0	6.5 ± 0.1	0.06
Aqp2	0.7 ± 0.4	0.5 ± 0.3	1.53
Aqp4	1.2 ± 0.1	0.4 ± 0.4	2.71
Hes1	3.3 ± 0.2	2.8 ± 1.0	1.18
CD68	0.7 ± 0.1	0.6 ± 0.2	1.26
PECAM	0.7 ± 0.2	3.5 ± 0.5	0.21
TGFB1	0.9 ± 0.1	1.27 ± 0.3	0.71

Mean ± SD Relative Quantitation (RQ) values (calibrated to UNFX) from quantitative real-time PCR analysis of 10^6 cells/sample are shown. Epithelial (E-cadherin), tubular (cubilin), collecting duct (Aqp2, Aqp4), glomerular (nephrin), vascular (KDR, PECAM), endocrine (erythropoietin), and other (Hes1, TGFB1, CD68) markers were compared.

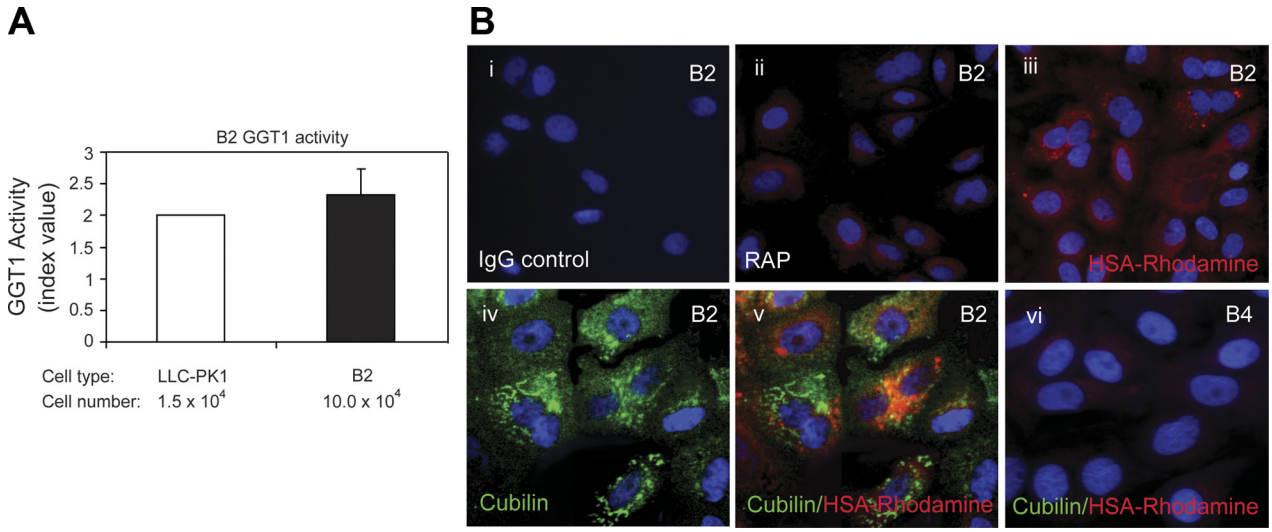

Fig. 2. Functional characterization of B2: γ-glutamyl transpeptidase (GGT1) activity and megalin:cubilin-mediated albumin transport. *A*: nitroaniline production from GGT1 measured as absorbance at 405 nm (A_{405}; mean ± SD) from 100,000 B2 cells and a reference standard of 15,000 LLC-PK1 cells. *B*: cubilin protein expression (green) and rhodamine-conjugated albumin uptake (red) assay. Nuclei were counterstained with Hoechst dye (blue). *i*: B2 cells stained with secondary antibody only. *ii*: Albumin uptake (red) after receptor-assisted protein (RAP) inhibition in B2 cells, *iii*: Albumin uptake (red) in B2 cells. *iv*: Cubilin expression (green) in B2 cells. *v*: Overlaid image showing colocalization of cubilin (green) and albumin (red) in B2 cells. *vi*: Albumin uptake (red) in nontubular B4 cells.

tubular cells and relative depletion of other cell types (vascular, glomerular) in B2 was confirmed by gene expression analysis (Table 7) of B2 in parallel with B4, a phenotypically distinct cell subpopulation that reproducibly sedimented at 1.073–1.091 g/ml and represented <2% of the UNFX cell input (1.4 ± 0.2% based on 5 independent preparations). Three gene targets, E-cadherin, cubilin, and aquaporin 4, were significantly enriched in B2 compared with both UNFX and the B4 population, supporting the tubular/collecting duct nature of the B2 fraction. The expression of Hairy enhancer of split-1 (*Hes-1*), a gene involved in mediation of Notch signaling with a potential role in tubular proliferation and regeneration (19), was also enriched in B2 compared with UNFX and B4.

Functional assays confirmed that the observed expression of GGT1 and cubilin resulted in active proteins. Nitroaniline was produced by active GGT1 in B2 cells (Fig. 2*A*), and fluorescently tagged albumin was actively transported into cubilin-positive B2 cells (Fig. 2*B*). Specificity of albumin transport was demonstrated by blockage with RAP, a known competitive inhibitor of megalin:cubilin-mediated albumin uptake (46), and by absence of transport in the nontubular B4 subpopulation (Fig. 2*B*).

In Vivo Bioactivity of UNFX and B2 in CKD Rodents

Two iterative studies were conducted to evaluate the efficacy of intrarenal delivery of UNFX and/or B2 cells to remnant

A. Study timeline

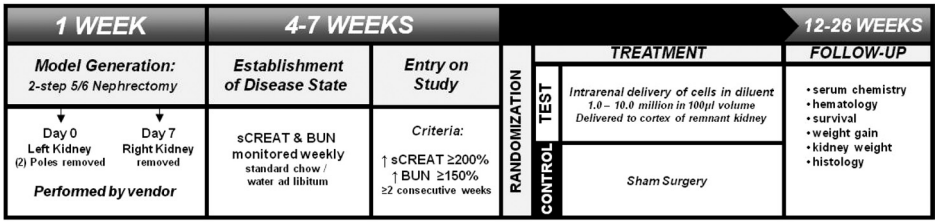

B. Pre-Treatment Entry Criteria Assessment

Study	Study A (6-month)			Study B (3-month)			Study B' (3-month)		
Total n	36			17			20		
	Non-NX rats (n=10)	NX rats (n=26)	Elevation %	Non-NX rats (n=10)	NX rats (n=7)	Elevation %	Non-NX rats (n=10)	NX rats (n=7)	Elevation %
sCREAT	0.3 ± 0.0	0.81 ± .23	270%	0.34 ± 0.05	0.74 ± 0.13	218%	0.35 ± 0.05	0.78 ± 0.16	222%
BUN	17.2 ± 1.8	35.0 ± 4.5	203%	18.2 ± 1.4	41.7 ± 5.4	229%	14.7 ± 1.2	36.6 ± 5.8	248%

C. Animal Assignment

	Non-NX rats		NX rats							
STUDY	No surg	SHAM	NX	UNFX LD (10^6)	UNFX HD (10^7)	B2 (10^7)	B2 ($5x10^6$)	B3-B4 ($5x10^6$)	Vehicle (cell-free)	TOTAL N
Study A	5	5	8	5	8	3	ND	ND	2	36
Study B	5	5	3	ND	ND	ND	4	ND	ND	17
Study B'	3	3	ND	ND	ND	ND	5	5	4	20

ND = not done

Fig. 3. Study timeline and design. *A*: timelines for model generation, treatment, and follow-up are presented along with criteria for study entry. *B*: age-, sex-, and batch-matched NX rats were confirmed to have ≥200% increase in serum creatinine (sCREAT) and ≥150% increase in blood urea nitrogen (BUN) relative to age- and sex-matched nonnephrectomized rats before treatment by serum chemistry in *studies A* and *B*. *C*: treatment groups, distribution of rats, and doses of UNFX and B2 for *studies A* and *B*.

kidneys of NX rats (Fig. 3). Treatment was initiated after progressive renal failure was established (persistent >200% elevation in sCREAT and >150% elevation in BUN). In *study A*, the heterogeneous UNFX cell population was delivered at high (10^7) and low (10^6) doses and compared with a high dose (10^7) of B2, untreated NX, and healthy Sham NX rats. Low-dose UNFX had a mild but transient survival benefit at 12 wk, or 90 days (Fig. 4*A*), but neither dose of UNFX significantly reduced the severity of disease present in the NX rats (Fig. 4*B*). In contrast to UNFX, treatment with B2 extended survival beyond the 90 day time point through study completion at 6 mo, or 180 days (Fig. 4*A*), and significantly improved systemic parameters associated with filtration function (sCREAT and BUN), protein handling (sALB and A:G), and general health (body weight) (Fig. 4*B*). Mild trends of improvement in erythropoiesis (Hct and hemoglobin) and mineral balance [serum phosphorus (sPHOS)] were also noted with B2 treatment but did not reach statistical significance at the 12 wk time point.

Study B was designed to confirm the in vivo effectiveness of B2 observed in *study A* in an independent experiment. A more physiologically relevant dose of B2 (5×10^6) was administered in *study B* to reduce the volume delivered into the remnant kidneys. B2 treatment in *study B* resulted in 100% survival (Fig. 4*A*) at 12 wk (90 days) and had stabilizing effects

A

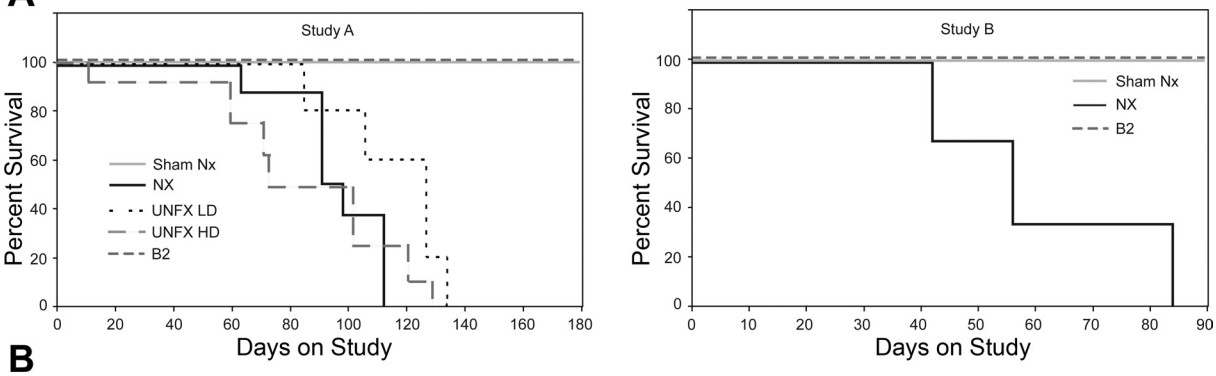

B

	Study A					Study B		
CLINICAL VALUE (12 WKS POST-TX)	Sham Nx	NX	UNFX LD	UNFX HD	B2	Sham Nx	NX	B2
GLOMERULAR FUNCTION								
SERUM CREATININE(mg/dl)	0.4 +/- 0.0	1.13 +/- 0.15	1.14 +/- 0.60	1.18 +/- 0.25	**0.70 +/- 0.10** **	0.4 +/- 0.7	2.23 +/- 0.46	**0.78 +/- 0.13** ***
BUN (mg/dl)	18.0 +/- 1.41	45.71 +/- 5.41	48.0 +/- 17.99	48 +/- 11.87	**36.33 +/- 7.77** *	18.80 +/-2.59	68.67 +/- 18.15	**34.00 +/- 3.56** *
TUBULAR FUNCTION								
SERUM ALBUMIN (g/dl)	4.22 +/- 0.08	2.84 +/- 0.10	2.66 +/- 0.23	2.83 +/- 0.10	**3.30 +/- 0.10** ***	3.84 +/- 0.18	2.67 +/- 0.31	2.80 +/- 0.22
A:G RATIO (A/G)	1.19 +/- 0.04	0.80 +/- 0.04	0.75 +/- 0.12	0.82 +/- 0.07	**1.05 +/- 0.12** **	1.16 +/- 0.07	0.78 +/- 0.13	0.76 +/- 0.10
CALCITRIOL FUNCTION								
SERUM PHOSPHOROUS (mg/dl)	4.58 +/- 0.25	4.69 +/- 0.60	5.84 +/- 2.67	5.48 +/- 0.92	4.37 +/- 0.40	7.94 +/- 2.07	8.33 +/- 3.64	5.98 +/- 0.52
SERUM CALCIUM (mg/dl)	8.93 +/- 0.67	8.98 +/- 1.91	8.62 +/- 3.04	7.53 +/- 2.61	9.13 +/- 0.12	11.20 +/- 0.44	12.10 +/- 0.98	11.65 +/- 0.21
ERYTHROPOIETIC FUNCTION								
HEMOGLOBIN (g/dl)	15.22 +/- 0.38	13.80 +/- 0.36	13.36 +/- 1.40	14.03 +/- 0.67	14.43 +/- 0.80	15.90 +/- 0.99	15.53 +/- 1.33	15.30 +/- 0.57
HEMATOCRIT (%)	46.94 +/- 1.18	42.67 +/- 1.92	41.62 +/- 3.99	43.13 +/- 0.99	44.73 +/- 1.44	47.70 +/- 5.35	45.00 +/- 5.07	44.28 +/- 2.21
WHOLE ORGANISM BENEFIT								
% Weight Gain	26.95 +/- 3.49	5.09 +/- 5.11	7.58 +/- 13.84	3.40 +/- 5.29	**12.24 +/- 2.16** *	9.11 +/- 19.14	5.2 +/- 12.1	1.03 +/- 3.93
Survival	100%	88%	100%	50%	100%	80%	0%	100%

C

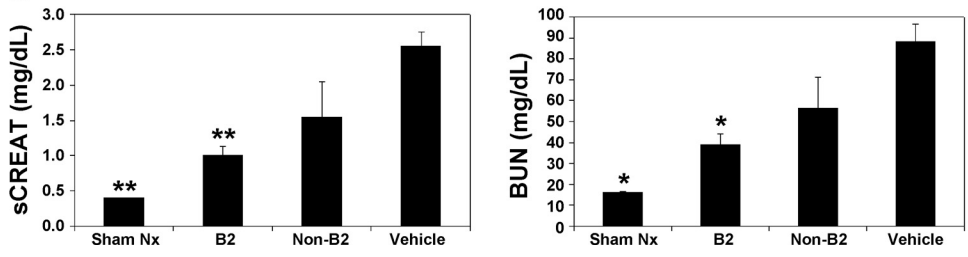

Fig. 4. UNFX and B2 effects on renal function and survival. *A*: survival plotted as % of rats surviving against days on study. *Day 0* marks delivery of treatment. Dotted lines represent untreated NX values from *study B*. LD dose; HD, high dose. *B*: serum chemistry values for all treatment groups (means ± SD) at 12 wk on study. Means are calculated from values obtained at 12 wk (surviving rats) or from preterminal blood draws (nonsurviving rats). *C*: direct comparison of the effects of B2 and non-B2 cells on filtration function in *study B′*. Mean ± SE sCREAT and BUN values obtained at 12 wk after treatment from Sham NX rats or NX rats treated with B2 ($n = 5$), non-B2 ($n = 5$), or vehicle ($n = 4$) are shown. Statistical significance: *$P < 0.05$ and ≥ 0.01; **$P < 0.01$ and ≥ 0.001; ***$P < 0.001$.

on sCREAT and BUN (Fig. 4*B*), nearly identical to those observed in *study A*. In contrast, 0% of NX rats survived 90 days. While trends of improvement were noted in other systemic parameters after B2 treatment in *study B* (e.g., sALB, sPHOS), statistical significance was not achieved (Fig. 4*B*).

Finally, the *study B* design was modified (*study B′*) to compare the observed systemic effects of B2 on renal filtration function to cell-free vehicle controls and to treatment with an equivalent dose (5×10^6) of non-B2 cells derived from the same UNFX starting population after density-gradient separation. At 12 wk after treatment, healthy Sham NX rats and B2 rats exhibited significantly lower sCREAT and BUN values compared with cell-free vehicle controls (Fig. 4*C*). While the non-B2 rats trended toward improvement in sCREAT and BUN, they remained statistically undifferentiated from vehicle controls. Consistent with the outcomes observed in *studies A* and *B*, the B2 group was characterized by 100% (5/5) survival 12 wk after implant, compared with 60% (3/5) for the non-B2 group and 50% (2/4) for the vehicle group.

B2-Mediated Augmentation of Renal Function in CKD Rodents

Disease progression in NX and B2 rats. Based on the reproducibility of B2 composition and in vivo bioactivity at two doses, remaining analyses focused on comparing B2 to diseased (NX) and healthy (Sham NX) rats. Temporal analysis of sCREAT and BUN from treatment through 6 mo showed that untreated NX rats experienced rapidly progressing kidney disease, reaching average sCREAT values >2.0 mg/dl and BUN values >65 mg/dl before death within 16 wk of study initiation. In contrast, B2 rats survived to study end point (24 wk) with significant stabilization of sCREAT and BUN beyond 10 wk of study (Fig. 5).

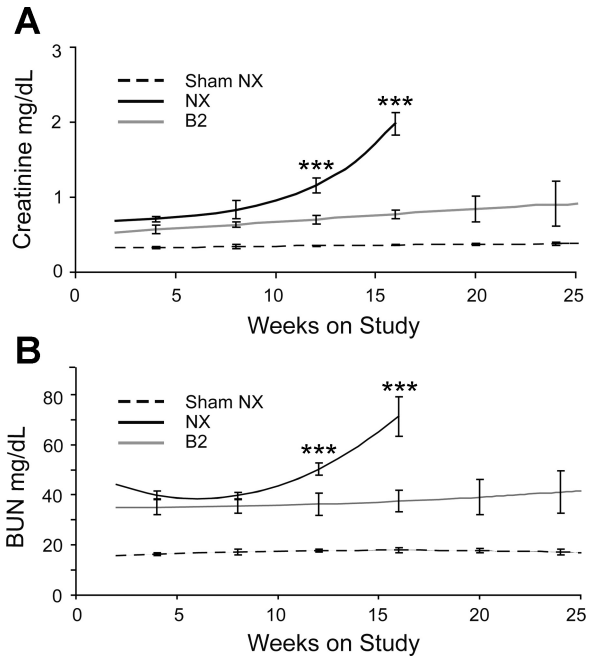

Fig. 5. Temporal analysis of sCREAT (*A*) and BUN (*B*). Significant differentiation in sCREAT between NX and B2 rats occurred after 10 wk posttreatment. ***$P < 0.001$.

Persistence of donor cell DNA at 6 mo after delivery. Remnant kidneys explanted at 24 wk were assayed to localize and quantify *SRY*+ DNA (Fig. 6). The majority of *SRY*+ donor-derived DNA persisted in the cortical/corticomedullary junction (CMJ) zone, at an estimated frequency of 1:33,333 cells. *SRY*+ DNA was found less frequently in the medullary zone, and no *SRY*+ was detected in the papillary/pelvic zone (Fig. 6*C*), suggesting that *SRY*+ cells are retained preferentially within the CMJ zone.

B2 effects on kidney tissue architecture. Sections of explanted kidney tissue were analyzed by semiquantitative histology to assess renal mass, glomerular injury, and tubulointerstitial injury (Fig. 7). NX kidneys were characterized by marked glomerular and tubulointerstitial injury, while B2-treated kidneys showed significantly less injury in comparison (Fig. 7*A*). At the time of death, NX remnant kidney weights were ~70% of healthy control kidneys, reflecting initial postnephrectomy compensation followed by progressive tissue degeneration. In contrast, remnant kidneys that received B2 were equivalent in mass to single kidneys from healthy Sham NX control rats (Fig. 7*B*). There was a strong inverse correlation between renal mass and sCREAT at the time of death [*P* value of 0.0092 ($\alpha = 0.05$)], suggesting that B2 treatment preserved and/or regenerated functional tissue mass.

High-magnification (×400) microscopy was used to examine major nephron compartments and semiquantitatively calculate glomerular and tubulointerstitial injury scores (Fig. 7, *C* and *D*). NX kidneys had multifocal to diffuse glomerular hypertrophy with segmental to global glomerular sclerosis, characterized by replacement of glomerular matrix with homogeneous eosinophilic material (protein), moderate mesangial proliferation, multifocal glomerular tuft adhesions, and focal glomerular atrophy. NX kidneys also exhibited mild to moderate tubulointerstitial fibrosis with multifocal inflammation. Multifocal tubular hypertrophy and hyperplasia existed predominantly in proximal tubules, and diffuse tubular dilatation affected both proximal and distal tubules. Most dilated tubules showed attenuated epithelium and thickened basement membrane, with many tubules containing hyaline casts indicating intraluminal protein accumulation. Kidneys from B2-treated rats had proportionally more healthy glomeruli, tubules, and nephron structures; minimal glomerular sclerosis; a decrease in tubular dilatation and hyaline casts; and a decrease in tubulointerstitial fibrosis (Fig. 7, *A*, *C*, and *D*). Although B2-treated rats had occasional foci of injured renal tissue evident within the parenchyma, the predominant morphology was consistent with that of Sham NX kidneys.

Histological evaluation of bone marrow and bone. Trends in erythropoietic functions associated with the NX model and B2 treatment, paired with the trends indicating reduced phosphatemia with B2 treatment at the 12 wk time point, prompted examination of the bone and bone marrow at the study end point (B2) or time of death (NX) (Fig. 8). NX bone marrow had reduced overall cellularity with a paucity of RBCs and increased myeloid-to-erythroid ratio. NX bone tissue had moderate resorption characterized by scalloping of endosteal surfaces with prevalent osteoclasts and the formation of lacunae, as well as thinning of the cortical and trabecular bone indicative of osteopenia. In contrast, B2 bone marrow had more free RBCs, homeostatic myeloid-to-erythroid ratios, and absence of histological evidence of bone resorption. Overall, the bone and

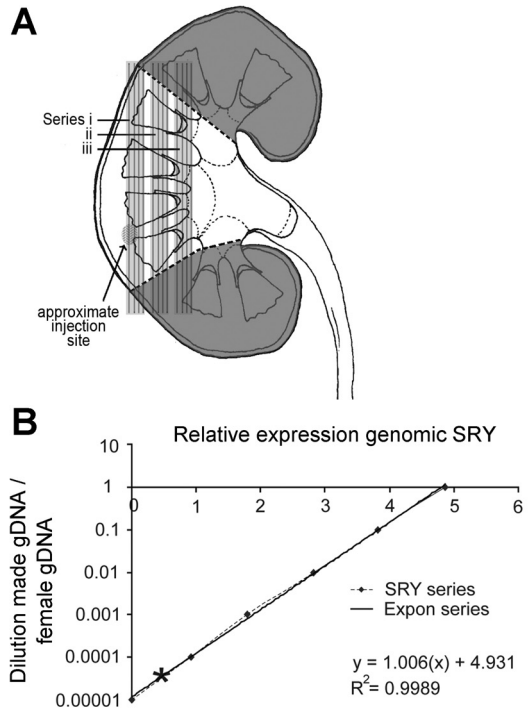

Fig. 6. Quantitative detection of donor male DNA in female host kidney 24 wk after B2 treatment. *A*: serial sections from kidney remnants of B2 rats in *study A* harvested at death (24 wk) and grouped into 3 series of 4 sections, each series totaling 20 μm of tissue. *Series i* spanned the cortex/corticomedullary junction zone (CMJ); *series ii* spanned the medulla; and *series iii* spanned the renal pelvis. Approximate site of injection is indicated. *B*: standard curve generated by plotting relative expression of SRY against dilution factor of controlled dilutions of male/female rat genomic DNA. Concentration of SRY in *series i* (CMJ) is indicated as forecast on the standard curve (*). *C*: estimated total of *SRY*-positive cells calculated from total gDNA isolated from each tissue series and *SRY* concentration with a standard value of 6.6 pg/DNA per diploid rodent cell (28).

C

Sample (20 microns)	Total sample gDNA (ng)	Forecasted SRY+ (% of total ng)	Total # cells in Sample (EST: 6.6 pg/cell)	SRY+ cells in Sample (EST: 6.6 pg/cell)
Series (i) CMJ	5,870	0.0030%	889,394	26.7
Series (ii) Medulla	2,060	0.0017%	312,121	4.4
Series (iii) Pelvis	3,810	0.0%	577,272	0.0

bone marrow of B2-treated rats approximated those of Sham NX (Fig. 8*A*).

Analysis of terminal serum phosphorus and calcium in Sham NX, B2, and NX rats corroborated histological findings. NX animals were hyperphosphatemic, consistent with osteodystrophy seen in end-stage renal disease (32). B2 treatment significantly reduced phosphorus levels relative to untreated NX animals (Fig. 8*B*), consistent with the histological findings in bone and bone marrow.

B2 Treatment Results in Modulation of Renal Fibrosis Pathways

Fibrosis represents a final common pathway of degeneration associated with CKD progression. A hallmark of fibrosis is the upregulation of profibrotic modulators such as transforming growth factor (TGF)-β1 (43) and plasminogen activator inhibitor (PAI)-1 (23), culminating in deposition of extracellular matrix (ECM) molecules such as fibronectin (FN) (14) in the interstitial spaces of glomeruli and tubules. On the basis of the histological observation that fibrotic changes associated with CKD progression in NX kidneys were abrogated in rats treated with B2, quantitative molecular analyses were conducted on B2-treated kidneys at the 3 and 6 mo time points and compared with study-matched diseased (NX) and healthy (Sham NX) controls. Quantitative analysis of gene expression for PAI-1, FN, and TGF-β1 provided evidence that the reduction in fibrotic change with B2 treatment was accompanied by clear attenuation of TGF-β1 expression (Fig. 9*B*). Consistent with gene expression, Western blot analysis demonstrated significant and progressive upregulation of PAI-1 in the NX kidneys and clear attenuation of PAI-1 expression in B2-treated kidneys (Fig. 9*A*). Significant reduction in FN production was also noted in B2-treated kidneys at the 6 mo time point (Fig. 9*A*). Taken together, these results suggest that B2 may impact fibrosis by modulation of pathways that affect ECM degradation (i.e., PAI-1) or deposition (i.e., TGF-β1) (Fig. 9*C*). Further studies are required to determine the details of this mechanism.

DISCUSSION

The goals of these iterative studies were to evaluate the therapeutic potential of a population of primary renal cells and to identify components of the population that were both therapeutically sufficient and technically reproducible. Intrarenal transplantation of unfractionated mixtures of renal cells (UNFX), containing tubular, glomerular, and endocrine components (1, 15), as well as other renal cell types, demonstrated partial efficacy in stabilizing renal function up to 3 mo after treatment, but the in vivo response to UNFX was inconsistent across most parameters, most notably survival, with only 4 of 15 UNFX-treated rats characterized by extended survival compared with the matched NX groups in their respective studies. In contrast, the enriched population of tubular cells (B2) provided consistent stabilization of renal filtration function, as evidenced by significantly lower sCREAT and BUN compared with matched NX controls. Surprisingly, the survival benefit associated with B2 treatment was far superior to UNFX, with

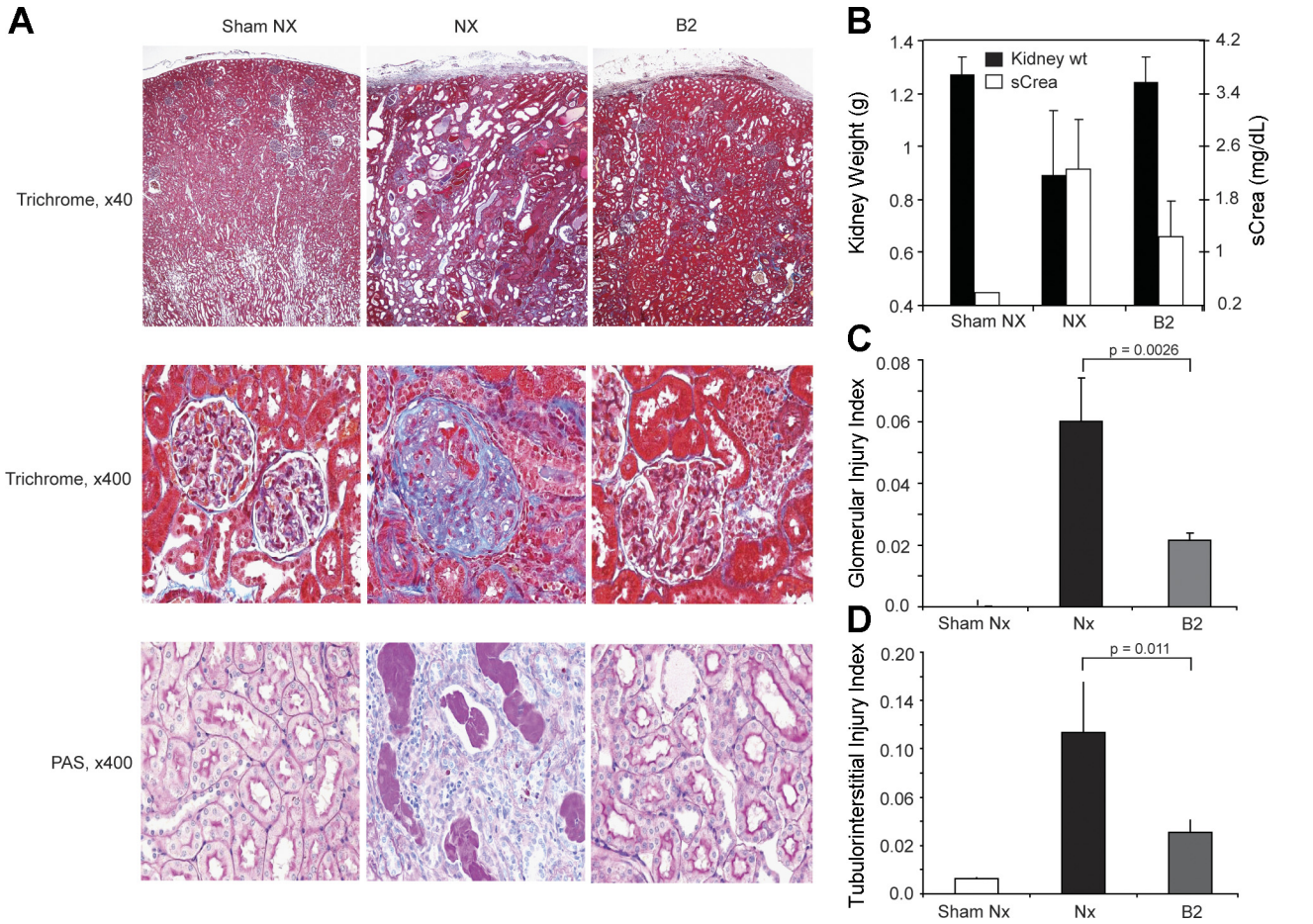

Fig. 7. Comparative renal histopathology 24 wk after B2 treatment. Samples are from Sham NX and B2 rats at 24 wk after treatment and the NX rat that survived to 16 wk on study. *A*: representative sections (stain indicated) from NX remnant kidney tissue show moderate to marked glomerular and tubulointerstitial injury, evidenced by glomerulosclerosis (trichrome), tubulointerstitial fibrosis (trichrome), and accumulation of protein casts in the tubular lumen [periodic acid Schiff (PAS)]. *B*: kidney weight and sCREAT values (sCrea) at necropsy. Posttreatment kidney weight was inversely proportional to sCREAT ($P = 0.0092$). *C* and *D*: standardized semiquantitative methods were used to generate indexes of glomerular injury (*C*) and tubulointerstitial injury (*D*). B2 treatment significantly reduced both glomerular and tubulointerstitial injury (*P* values indicated).

12 of 12 rats surviving 3 mo after treatment and 3 of 3 surviving to the study end point of 6 mo. Qualitative and quantitative histopathological assessment provided clear confirmation of systemic effects at the tissue level, with B2 treatment leading to significant reductions in both glomerular and tubulointerstitial injury.

Before initiation of *studies A* and *B*, work was completed to examine the suitability of the two-step 5/6 nephrectomy as a terminally progressive model of renal failure. As indicated by published literature (26), we found that a two-step 5/6 surgical reduction in renal mass provided a reproducible reduction in filtration and progressive uremia, as evidenced by consistent >200% increases in sCREAT and BUN within 4–7 wk of model generation. Importantly, among the 15 NX rats utilized in these studies (proof of concept, *study A*, and *study B*), there was no spontaneous recovery or nonprogressive stabilization—100% of the NX rats had progressive elevations in sCREAT and BUN from the time of model generation until the time of death. Additional preliminary work demonstrated that cultured renal cells (UNFX) could be injected into the remnant kidney parenchyma after onset of overt disease, via cortical access at a depth approximating the corticomedullary junction. Cellular distribution and persistence of male UNFX cells, labeled before implantation with a red fluorescent membrane-intercalating dye (PKH26), was examined 4 wk after implantation, and the cells were found to be moderately distributed throughout the remnant kidney, with greater cell presence proximal to the injection site. Close examination of B2-treated remnant kidney sections probed for Y chromosome via FISH revealed that Y+ donor cells persisted for at least 3 mo after implant and were localized in general to the tubular and peritubular space in the corticomedullary zone. PCR-based detection of *SRY*, a Y chromosome-localized gene that has been used to assess chimerism in transplantation studies (16), confirmed retention of donor cell-derived male DNA in the female recipient tissue and provided support for quantitative adaptation of *SRY* detection for subsequent studies. However, neither membrane dye nor *SRY* detection elucidates the mechanisms of retention (e.g., individual incorporated cells or fusion products with host cells).

Because the kidney is a complex organ comprised of >20 cell types (33), we initially postulated that a complex mixture of cell types (i.e., UNFX) would be required to achieve therapeutically relevant regeneration of a diseased kidney.

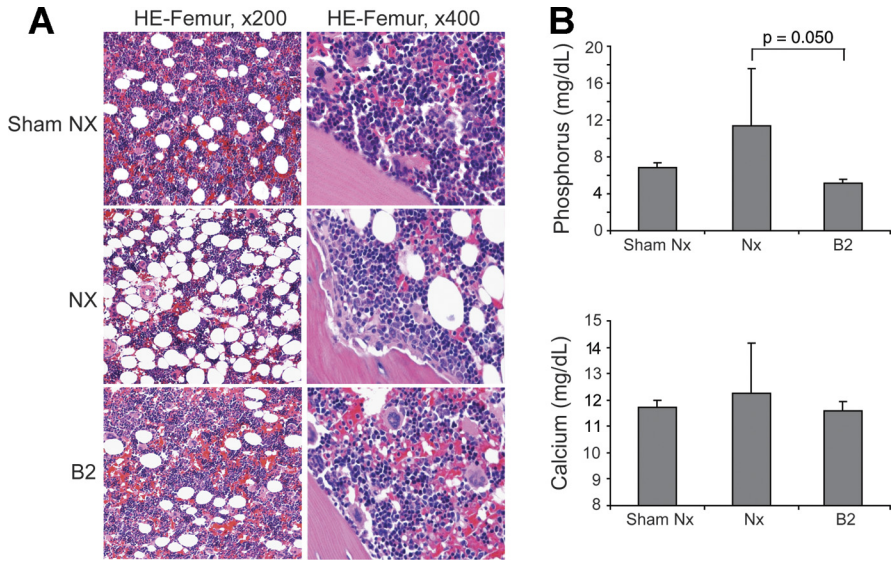

Fig. 8. Bone marrow, bone tissue, and calcium:phosphorus balance. *A*: hematoxylin and eosin (HE)-stained sections from femurs collected at necropsy (Sham NX and B2: 24 wk; NX: 16 wk). Compared with healthy Sham NX, the bone marrow of NX rats had a paucity of red blood cells and an increased myeloid-to-erythroid ratio, as well as scalloping of endosteal surfaces with prevalent osteoclasts, formation of lacunae, and thinning of the cortical and trabecular bone. The marrow and bone tissue of B2-treated rats approximated that of healthy Sham NX rats. *B*: serum phosphorus and calcium levels from prenecropsy blood draws (24 wk on study). NX rats were hyperphosphatemic, yet B2 rats had phosphorus levels within the range of those seen in Sham NX rats ($P > 0.05$) and significantly lower than NX rats ($P = 0.05$) with exclusion of one outlier value in the NX group (serum phosphorous = 24.3 mg/dl; > 2 standard deviations from the mean). Calcium homeostasis was maintained in all treatment groups.

Numerous studies on regeneration of renal architecture and function following acute kidney injury point to tubular epithelial cells as playing a key role in restoring function (10, 21); we therefore sought to compare a population of renal epithelial cells that were predominantly tubular and relatively depleted of other cell types (vascular, glomerular, endocrine, and undefined cell types) to the more heterogeneous UNFX mixture. Tubular cells can be separated from other kidney cell types on the basis of differential buoyant density (20); thus we adapted and optimized density-gradient centrifugation methods for postculture population fractionation of UNFX. The predominant population of tubular cells reproducibly separated from the remaining cells as a well-defined band (B2) with buoyant density between 1.045 and 1.063 g/ml and was tested initially as an epithelial cell-enriched control comprised of tubular and some aquaporin 2-positive collecting duct cells (Table 6). The in vivo performance of B2 compared with UNFX was somewhat unexpected but can be aligned with the aforementioned capacity of the tubular cell compartment to participate in the regenerative response after injury (10, 21). The UNFX population contains an ample number of tubular cells; however, it also contains large cells of the collecting duct system, glomerular cells, vascular cells, endocrine cells, and other undefined cell types. When this is paired with the observation that a low dose of UNFX provided an outcome superior to a high dose of UNFX, it is not unreasonable to postulate that the superior performance of B2 compared with UNFX may be due in part to the absence of specific cellular components. This hypothesis is also supported by the observed heterogeneity in response to UNFX treatment (Table 5 and Fig. 4). Other fractional components of UNFX, when tested at a dose equivalent to B2 (non-B2 in *study B′*), failed to provide the systemic and survival benefits of B2, suggesting that specific cellular components of B2 are required to achieve a therapeutic outcome in this model of CKD. However, this observation does not preclude the possibility that non-B2 components of UNFX could act synergistically with B2 to achieve a regenerative outcome.

It is of importance to note that nonembryonic kidney-derived parenchymal cells have not been evaluated previously for therapeutic efficacy in chronic, progressive models of renal failure. It is also important to distinguish that the B2 population provided clear and consistent therapeutic benefit in both the initial study (*study A*) and the follow-on studies (*studies B* and *B′*), even though treatment was delivered only after a consistent >200% elevation in sCREAT and BUN was achieved in the model. The employment of "enrollment criteria" in these studies and intervention only after a chronic disease state was established are key distinctions from studies of cell-based treatments for acute renal injury, where cells are often delivered at the same time of insult or immediately thereafter (22, 27).

The most consistently altered systemic parameters across the studies were sCREAT and BUN, both of which climbed to >200% of baseline before treatment and, in untreated NX rats, continued to climb until death. Treatment with B2 consistently and significantly improved survival and stabilized key biomarkers of renal filtration function—sCREAT and BUN (Figs. 4, 5). Studies of acute renal failure have provided evidence that regeneration and repair within the tubular compartment can impact physiological parameters throughout the kidney (13), which can be driven by mechanisms such as tubuloglomerular feedback (38) or paracrine actions (13).

Other functional parameters showed biological trends but did not consistently achieve statistical significance; these included parameters that assess protein handling by the nephron (sALB and A:G), parameters indicating erythropoietic function (hemoglobin and Hct), whole organism level indicators (weight gain), and indicators of calcitriol- and parathyroid hormone (PTH)-mediated mineral homeostasis (serum calcium and phosphorus). Interestingly, as highlighted in Fig. 8*B*, the trend toward reduced phosphatemia observed 3 mo after treatment (Fig. 4*B*) was significant ($P = 0.05$) at the 6 mo time point (Fig. 8*B*), with sPHOS levels in B2-treated rats equivalent to those in healthy Sham NX rats, likely reflecting improvements in GFR and potentially involving production of active vitamin D by the kidney to facilitate the proper absorption of calcium and phosphorus (12). The absence of bone erosion and osteoclastic lesions in the femoral bone of B2-treated rats relative to NX rats supports the systemic observation that phosphatemia is attenuated with treatment. Additional analyses are

A

Group / Marker	Study B (12 week study)		Study A (24 week study)	
	NX	B2	NX	B2
TGFβ1	0.1178 ± 0.119	0.0358 ± 0.011	0.1200 ± 0.050	0.0505 ± 0.008**
PAI-1	0.3591 ± 0.273	0.0653 ± 0.015*	0.2459 ± 0.046	0.0749 ± 0.022***
FN	0.0308 ± 0.015	0.0108 ± 0.003*	0.1281 ± 0.088	0.0460 ± 0.016*

B

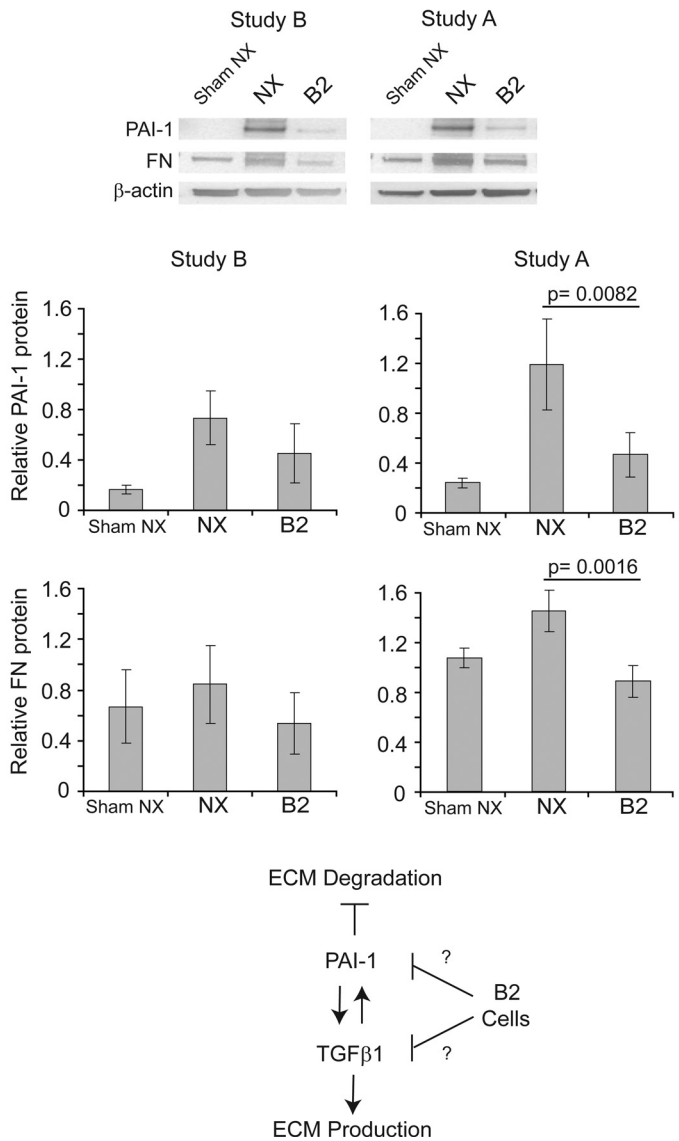

C

Fig. 9. B2 treatment attenuates transforming growth factor (TGF)-β1, plasminogen activator inhibitor (PAI)-1, and fibronectin (FN) expression in vivo. *A*: relative gene quantitation values for TGF-β1, PAI-1, and FN at necropsy were normalized to time on study to generate a slope value representing the rate of change in gene expression per animal. Reported values are means ± SD for NX and B2 groups. Statistical significance: $*P < 0.05$ and ≥ 0.01; $**P < 0.01$ and ≥ 0.001; $***P < 0.001$. *B*: Western blot analysis (representative blot) and semiquantitative densitometry (all samples) of PAI-1, FN, and β-actin proteins at 12 (*study B*) and 24 (*study A*) wk after B2 treatment. Statistically significant reductions in PAI-1 and FN are observed at 24 wk in B2-treated rats (*P* values indicated). *C*: potential mechanism whereby B2 treatment may directly or indirectly affect the PAI-1/TGF-β1 positive feedback loop to inhibit extracellular matrix (ECM) production and/or enhance ECM degradation in vivo.

required to evaluate the effects of B2 treatment on mediators of calcium/phosphorus homeostasis. (e.g., renal vitamin D-24-hydroxylase, calcitriol, and PTH) and elucidate the mechanism(s) involved.

Histological findings in the remnant kidneys corroborated the systemic results, demonstrating that B2-treated rats had significantly lower glomerular injury and tubulointerstitial injury scores than NX rats. Glomerular and tubulointerstitial fibrosis were clearly attenuated with B2 treatment, an affect that was apparent and measurable a full 6 mo after treatment—3 mo beyond the time that the untreated NX rats died. Also notable in B2-treated remnant kidneys was the significant reduction in intraluminal protein casts, suggesting a treatment-induced improvement in protein handling by the nephron. Systemic data showing significant improvements in serum protein and A:G in Fig. 4*B* support the conclusion that treatment with B2 improves protein handling, by reducing leakage of protein into the glomerular filtrate and/or enhancing protein resorption along the tubules.

Progressive fibrosis is a hallmark of CKD and is a clear feature of the 5/6 NX model. The accumulation of fibrotic ECM proteins, which include FN and type I collagen, has long been associated with persistent expression of TGF-β1 by injured or distressed cells (2). Additionally, the inhibition of

plasmin-dependent proteolysis of ECM proteins, through the increased expression of PAI-1, can further promote the development of fibrotic lesions (8). Recently, it has been shown that TGF-β1 and PAI-1 participate in a positive feedback loop that, when left unchecked, can lead to the cumulative effects of increased ECM deposition and insufficient ECM degradation (36). Molecular analyses of kidney tissue at the time of necropsy (3 and 6 mo after treatment) show clearly that treatment with B2 attenuated expression of TGF-β1, PAI-1, and FN (Fig. 9). While it is still uncertain whether this effect is through direct or indirect mechanisms, it is tempting to speculate that B2 cells are communicating to host cells through paracrine factors. This hypothesis is supported, in part, by the observation that the reduction in profibrotic markers is maintained even 6 mo after implantation, despite the relatively low number of donor cells as detected by *SRY* in those same tissues. Further studies are being conducted to identify key factors that may account for the antifibrotic properties of implanted B2 cells.

The data presented here show clearly that B2 stimulates regeneration in the remnant kidney, stabilizes renal function, and enhances survival, with the effects being more pronounced and more durable than has been reported with other cell-based approaches to the treatment of kidney disease (6, 9, 18, 45), the majority of which have focused on the treatment of acute renal failure. Of the limited studies that examined cell-based interventions in chronic disease models, none has tracked as wide a range of systemic parameters and histology as the studies described here or demonstrated 6-mo durability of effect (5, 31, 44). The mechanism(s) by which B2 functions in this model is likely to consist of a complex combination of direct effects (cell-mediated functions) and indirect effects (paracrine functions). Compartment-specific assessment of cellular engraftment and delineation between direct and indirect effects will require follow-up lineage-tracing studies that enable implanted B2 cells to be reliably identified and phenotyped. In these initial studies, we have taken advantage of the syngeneic Lewis model to deliver male cells (carrying *SRY* on the Y chromosome) to female hosts, enabling quantitative detection of the ratio of male to female DNA by quantitative PCR. As highlighted in Fig. 6, longitudinal serial sections were made through the kidney, and the relative presence of *SRY* was assessed in the CMJ zone, the medullary zone, and the renal pelvis zone, with the CMJ zone showing the greatest retention of male cells at the 6 mo time point, estimated to be 1:33,333 cells. These results provide evidence against clonal expansion of implanted cells, which has been noted in cell-based approaches to genetic models of kidney damage (11). The data suggest instead that a relatively small number of B2 cells can stimulate a regenerative process that sustainably alters the disease process at the tissue level.

These studies have demonstrated that regenerative therapies for CKD can be comparatively evaluated in vivo for efficacy and durability with the NX model. B2 exhibited the potential for long-term protection and restoration of cellular and tissue function associated with the major renal compartments: tubules and glomeruli. Collectively, these data indicate that renal cell subpopulations having specific in vitro functional attributes can restore homeostatic tissue architecture and prevent or delay progression of CKD. The strategy of treating NX rats after sCREAT had doubled was analogous to treating a CKD patient after a progressive disease state is established but before renal failure has progressed to end-stage disease, requiring dialysis or whole organ transplantation. These results provide proof of concept that interventional regenerative strategies could slow progression of CKD, thereby delaying the need for dialysis or reducing the frequency of dialysis required in CKD patients. Further translation of these therapeutic concepts will require assessment of efficacy in the context of comorbid diseases, such as diabetes and hypertension.

DISCLOSURES

All authors are employees of Tengion, Inc. except for H. S. Rapoport and P. Tatsumi-Ficht, who left the company after the completion of this work.

REFERENCES

1. **Aboushwareb T, Egydio F, Straker L, Gyabaah K, Atala A, Yoo JJ.** Erythropoietin producing cells for potential cell therapy. *World J Urol* 26: 295–300, 2008.
2. **Border WA, Noble NA.** Transforming growth factor beta in tissue fibrosis. *N Engl J Med* 331: 1286–1292, 1994.
3. **Brenner BM.** Nephron adaptation to renal injury or ablation. *Am J Physiol Renal Fluid Electrolyte Physiol* 249: F324–F337, 1985.
4. **Caruso-Neves C, Kwon SH, Guggino WB.** Albumin endocytosis in proximal tubule cells is modulated by angiotensin II through an AT2 receptor-mediated protein kinase B activation. *Proc Natl Acad Sci USA* 102: 17513–17518, 2005.
5. **Chade AR, Zhu X, Lavi R, Krier JD, Pislaru S, Simari RD, Napoli C, Lerman A, Lerman LO.** Endothelial progenitor cells restore renal function in chronic experimental renovascular disease. *Circulation* 119: 547–557, 2009.
6. **Choi S, Park M, Kim J, Hwang S, Park S, Lee Y.** The role of mesenchymal stem cells in the functional improvement of chronic renal failure. *Stem Cells Dev* 18: 521–529, 2009.
7. **DeLisser HM, Christofidou-Solomidou M, Strieter RM, Burdick MD, Robinson CS, Wexler RS, Kerr JS, Garlanda C, Merwin JR, Madri JA, Albelda SM.** Involvement of endothelial PECAM-1/CD31 in angiogenesis. *Am J Pathol* 151: 671–677, 1997.
8. **Eddy AA, Fogo AB.** Plasminogen activator inhibitor-1 in chronic kidney disease: evidence and mechanisms of action. *J Am Soc Nephrol* 17: 2999–3012, 2006.
9. **Eliopoulos N, Gagnon RF, Francois M, Galipeau J.** Erythropoietin delivery by genetically engineered bone marrow stromal cells for correction of anemia in mice with chronic renal failure. *J Am Soc Nephrol* 17: 1576–1584, 2006.
10. **Guo JK, Cantley LG.** Cellular maintenance and repair of the kidney. *Annu Rev Physiol* 72: 357–376, 2010.
11. **Held PK, Al-Dhalimy M, Willenbring H, Akkari Y, Jiang S, Torimaru Y, Olson S, Fleming WH, Finegold M, Grompe M.** In vivo genetic selection of renal proximal tubules. *Mol Ther* 13: 49–58, 2006.
12. **Hercz G.** Regulation of bone remodeling: impact of novel therapies. *Semin Dial* 14: 55–60, 2001.
13. **Humes HD, Lake EW, Liu S.** Renal tubule cell repair following acute renal injury. *Miner Electrolyte Metab* 21: 353–365, 1995.
14. **Jones CL, Buch S, Post M, McCulloch L, Liu E, Eddy AA.** Renal extracellular matrix accumulation in acute puromycin aminonucleoside nephrosis in rats. *Am J Pathol* 141: 1381–1396, 1992.
15. **Joraku A, Stern KA, Atala A, Yoo JJ.** In vitro generation of three-dimensional renal structures. *Methods* 47: 129–133, 2009.
16. **Kakinoki R, Bishop AT, Tu YK, Matsui N.** Detection of the proliferated donor cells in bone grafts in rats, using a PCR for a Y-chromosome-specific gene. *J Orthop Sci* 7: 252–257, 2002.
17. **Kaufman JM, DiMeola HJ, Siegel NJ, Lytton B, Kashgarian M, Hayslett JP.** Compensatory adaptation of structure and function following progressive renal ablation. *Kidney Int* 6: 10–17, 1974.
18. **Kim SS, Park HJ, Han J, Gwak SJ, Park MH, Song KW, Rhee YH, Min Chung H, Kim BS.** Improvement of kidney failure with fetal kidney precursor cell transplantation. *Transplantation* 83: 1249–1258, 2007.
19. **Kobayashi T, Terada Y, Kuwana H, Tanaka H, Okado T, Kuwahara M, Tohda S, Sakano S, Sasaki S.** Expression and function of the Delta-1/Notch-2/Hes-1 pathway during experimental acute kidney injury. *Kidney Int* 73: 1240–1250, 2008.

20. **Kreisberg JI, Pitts AM, Pretlow TG.** Separation of proximal tubule cells from suspensions of rat kidney cells in density gradients of Ficoll in tissue culture medium. *Am J Pathol* 86: 591–602, 1977.
21. **Lin F, Moran A, Igarashi P.** Intrarenal cells, not bone marrow-derived cells, are the major source for regeneration in postischemic kidney. *J Clin Invest* 115: 1756–1764, 2005.
22. **Mazzinghi B, Ronconi E, Lazzeri E, Sagrinati C, Ballerini L, Angelotti ML, Parente E, Mancina R, Netti GS, Becherucci F, Gacci M, Carini M, Gesualdo L, Rotondi M, Maggi E, Lasagni L, Serio M, Romagnani S, Romagnani P.** Essential but differential role for CXCR4 and CXCR7 in the therapeutic homing of human renal progenitor cells. *J Exp Med* 205: 479–490, 2008.
23. **Nakamura S, Nakamura I, Ma L, Vaughan DE, Fogo AB.** Plasminogen activator inhibitor-1 expression is regulated by the angiotensin type 1 receptor in vivo. *Kidney Int* 58: 251–259, 2000.
24. **Nelson WJ, Shore EM, Wang AZ, Hammerton RW.** Identification of a membrane-cytoskeletal complex containing the cell adhesion molecule uvomorulin (E-cadherin), ankyrin, and fodrin in Madin-Darby canine kidney epithelial cells. *J Cell Biol* 110: 349–357, 1990.
25. **Oosterwijk E, Van Muijen GN, Oosterwijk-Wakka JC, Warnaar SO.** Expression of intermediate-sized filaments in developing and adult human kidney and in renal cell carcinoma. *J Histochem Cytochem* 38: 385–392, 1990.
26. **Ormrod D, Miller T.** Experimental uremia. Description of a model producing varying degrees of stable uremia. *Nephron* 26: 249–254, 1980.
27. **Patschan D, Krupincza K, Patschan S, Zhang Z, Hamby C, Goligorsky MS.** Dynamics of mobilization and homing of endothelial progenitor cells after acute renal ischemia: modulation by ischemic preconditioning. *Am J Physiol Renal Physiol* 291: F176–F185, 2006.
28. **Peterson DG, Stack SM, Healy JL, Donohoe BS, Anderson LK.** The relationship between synaptonemal complex length and genome size in four vertebrate classes (Osteicthyes, Reptilia, Aves, Mammalia). *Chromosome Res* 2: 153–162, 1994.
29. **Platt R, Roscoe MH, Smith FW.** Experimental renal failure. *Clin Sci (Lond)* 11: 217–231, 1952.
30. **Powe NR, Plantinga L, Saran R.** Public health surveillance of CKD: principles, steps, and challenges. *Am J Kidney Dis* 53: S37–S45, 2009.
31. **Prodromidi EI, Poulsom R, Jeffery R, Roufosse CA, Pollard PJ, Pusey CD, Cook HT.** Bone marrow-derived cells contribute to podocyte regeneration and amelioration of renal disease in a mouse model of Alport syndrome. *Stem Cells* 24: 2448–2455, 2006.
32. **Ritz E.** The clinical management of hyperphosphatemia. *J Nephrol* 18: 221–228, 2005.
33. **Rosines E, Johkura K, Zhang X, Schmidt HJ, Decambre M, Bush KT, Nigam S.** Constructing kidney-like tissues from cells based on programs for organ development: towards a method of in vitro engineering of the kidney. *Tissue Eng Part A* 16: 2441–2455, 2010.
34. **Sasaki S, Noda Y.** Aquaporin-2 protein dynamics within the cell. *Curr Opin Nephrol Hypertens* 16: 348–352, 2007.
35. **Sellers RS, Morton D, Michael B, Roome N, Johnson JK, Yano BL, Perry R, Schafer K.** Society of Toxicologic Pathology position paper: organ weight recommendations for toxicology studies. *Toxicol Pathol* 35: 751–755, 2007.
36. **Seo JY, Park J, Yu MR, Kim YS, Ha H, Lee HB.** Positive feedback loop between plasminogen activator inhibitor-1 and transforming growth factor-beta1 during renal fibrosis in diabetes. *Am J Nephrol* 30: 481–490, 2009.
37. **Shackelford C, Long G, Wolf J, Okerberg C, Herbert R.** Qualitative and quantitative analysis of nonneoplastic lesions in toxicology studies. *Toxicol Pathol* 30: 93–96, 2002.
38. **Singh P, Thomson SC.** Renal homeostasis and tubuloglomerular feedback. *Curr Opin Nephrol Hypertens* 19: 59–64, 2010.
39. **Takata K, Matsuzaki T, Tajika Y, Ablimit A, Hasegawa T.** Localization and trafficking of aquaporin 2 in the kidney. *Histochem Cell Biol* 130: 197–209, 2008.
40. **Tate SS, Meister A.** gamma-Glutamyl transpeptidase from kidney. *Methods Enzymol* 113: 400–419, 1985.
41. **Terryn S, Jouret F, Vandenabeele F, Smolders I, Moreels M, Devuyst O, Steels P, Van Kerkhove E.** A primary culture of mouse proximal tubular cells, established on collagen-coated membranes. *Am J Physiol Renal Physiol* 293: F476–F485, 2007.
42. **U.S. Renal Data System.** Minneapolis, MN: U.S. Renal Data System, 2007.
43. **Wu LL, Cox A, Roe CJ, Dziadek M, Cooper ME, Gilbert RE.** Transforming growth factor beta 1 and renal injury following subtotal nephrectomy in the rat: role of the renin-angiotensin system. *Kidney Int* 51: 1553–1567, 1997.
44. **Yuen DA, Connelly KA, Advani A, Liao C, Kuliszewski MA, Trogadis J, Thai K, Advani SL, Zhang Y, Kelly DJ, Leong-Poi H, Keating A, Marsden PA, Stewart DJ, Gilbert RE.** Culture-modified bone marrow cells attenuate cardiac and renal injury in a chronic kidney disease rat model via a novel antifibrotic mechanism. *PLoS One* 5: e9543, 2010.
45. **Zeisberg M, Strutz F, Muller GA.** Renal fibrosis: an update. *Curr Opin Nephrol Hypertens* 10: 315–320, 2001.
46. **Zhai XY, Nielsen R, Birn H, Drumm K, Mildenberger S, Freudinger R, Moestrup SK, Verroust PJ, Christensen EI, Gekle M.** Cubilin- and megalin-mediated uptake of albumin in cultured proximal tubule cells of opossum kidney. *Kidney Int* 58: 1523–1533, 2000.